water

MDPI

Article

Reconstruction of Groundwater Level Data Using Temporal Components of Groundwater Fluctuations Based on Wavelet Analysis and Artificial Neural Networks

Oleksii Shevchenko [1,*], Dmytro Charnyi [2], Ilya Zaslavsky [3], Vytautas Samalavičius [4] and Yuliia Sovkova [1]

1 Ukrainian Hydrometeorological Institute NAS of Ukraine, Nauki Av., 37, 03028 Kyiv, Ukraine; juliiasovkova@gmail.com
2 Institute of Environmental Geochemistry NAS of Ukraine, Akademika Palladina Avenue, 34-a, 03142 Kyiv, Ukraine; dmitriych10@gmail.com
3 Spatial Information Systems Laboratory, San Diego Supercomputer Center, University of California San Diego, 9836 Hopkins Drive, La Jolla, CA 92093, USA; izaslavsky@ucsd.edu
4 Institute of Geosciences, Faculty of Chemistry and Geosciences at Vilnius University, Čiurlionio Str. 21/27, 03101 Vilnius, Lithuania; vytautas.samalavicius@chgf.vu.lt
* Correspondence: shevch62@gmail.com

Abstract

Since the observations of groundwater level (GWL) in Ukraine are not conducted by automated means, the regularity of the data is affected by the human factor as well as social unrest. Since 2022, this has been a full-scale war launched by the russian federation. Continuous long-term GWL observations (to 2011, sometimes until 2017) were used to reconstruct periods with missing measurements, combining autocorrelation analysis, wavelet decomposition, Mann–Kendall trend testing, and artificial neural networks (ANNs). The strongest reconstruction performance was achieved by separating GWL fluctuations into short-, medium-, and long-period components and modeling the dominant medium- and long-period structures. Compared with linear autoregressive baselines, multilayer perceptrons (MLPs) better approximated nonlinear relationships present in the historical record. At the same time, these data-driven models remain sensitive to nonstationarity and should be interpreted as predictive tools rather than causal process models. The data reconstruction study covers the transboundary basin of the Bug River, which is significant for Ukraine and Poland as a water resource.

Keywords: groundwater level; artificial neural networks; wavelet analysis; reconstruction; multilayer perceptrons; Western Bug basin

Academic Editor: Juan José Durán

Received: 8 May 2026
Revised: 9 August 2026
Accepted: 20 August 2026
Published: 26 August 2026

1. Introduction

The availability and quality of groundwater monitoring data vary substantially across transboundary river basins, complicating water-resource assessment and coordination of management decisions between neighboring countries. A representative case is the Western Bug River basin (Western Bug in Ukrainian usage; Bug in Polish usage). In Poland, automated groundwater observations and dense watershed monitoring networks support robust verification of satellite products [1,2]. In Ukraine, however, the monitoring network is sparse, and many observation series were discontinued from 2013 to 2022, substantially limiting regional assessment of drinking groundwater resources (see Figure S1). At present, routine monitoring in Ukraine mainly covers river discharge and groundwater abstraction exceeding 300 m^3/day, or water extraction for commercial use regardless of volume. In

 https://doi.org/10.3390/w18172105

the context of ongoing russian attacks on civilian life support infrastructure, including water intakes, timely information on groundwater-level fluctuations and drinking-water source status is critical for public safety. Accordingly, monitoring should include not only exploited aquifers in central and western Ukraine, where internal population displacement has increased demand, but also shallow groundwater, which recharges operational aquifers and is more sensitive to adverse climate variability.

Because hydrogeological drought is difficult to quantify without continuous monitoring, regional assessments can use GRACE (Gravity Recovery and Climate Experiment) and its successor mission GRACE-FO (Follow-On) satellite products [3,4]. However, satellite-based estimates still require validation against in situ groundwater table observations. Therefore, it is necessary to reconstruct realistic GWL values at representative locations from the beginning of the cessation of observations to the present time. This problem can be addressed through the application of artificial intelligence (AI) techniques, including machine learning (ML) and deep learning (DL) approaches such as artificial neural networks (ANNs).

ANN models are widely used to model and forecast hydrological and hydrogeological variables, including river discharge, groundwater levels, and water quality [5,6]. Feedforward backpropagation (FFBP) networks are commonly applied to complex hydrological prediction tasks. A study on a regional-scale dataset of GWL imputations proved to be successful [7]. For monthly groundwater-level modeling [8], recurrent neural networks (RNN), multilayer perceptrons (MLP), and radial basis function networks (RBF) have all been used. For unconfined Cretaceous aquifer levels in northern France, a case similar to ours, Lallahem et al. [9] reported good performance of MLP models. A study by [10] reveals that DL models are frequently more accurate in predictions compared to traditional models. Because ANN methods are empirical, their reliability depends strongly on data quality, temporal representativeness, and consistency between training and forecasting conditions.

In most studies, groundwater levels are predicted using local explanatory variables considered to control fluctuations under specific site conditions. Frequently used predictors include precipitation, air temperature, potential evapotranspiration, groundwater abstraction, nearby drainage levels and discharge, reservoir inflow, irrigation coefficients, and irrigated area, soil moisture, GRACE-derived groundwater storage (GWS) [8,9,11–15]. Recent studies have shown that machine-learning approaches can improve groundwater-level estimation by combining monitoring data with hydroclimatic and remotely sensed predictors [15,16]. These methods are particularly useful in data-scarce regions, where groundwater dynamics are non-linear and monitoring networks are often sparse. Recent work has also demonstrated the value of hybrid approaches that combine machine learning models with simulation outputs to forecast groundwater storage under limited data availability [17]. In the Baltic region, data-driven approaches have shown potential for groundwater level gap imputation and sinkhole-risk forecasting, while also indicating that model performance depends strongly on gap length, predictor availability, and local hydrogeological variability [7,18].

Autocorrelation-based forecasting often requires long datasets for training and validation [19,20]. Autoregressive models [21] assume that the current state depends on previous states, with error and seasonality terms [22]. In practice, these approaches may smooth extreme events and underestimate minima and maxima.

Given the limited recent observations and the likely anomalously low groundwater-table recession in 2019–2020, we need model configurations that can reproduce long-term GWL dynamics with high fidelity, support basin-scale extrapolation, and improve satellite-data validation.

The aim of this study is to fill observational gaps and identify key trends in GWL changes following the cessation of monitoring in the transboundary Western Bug basin (Figure 1) within Lviv Region, using available hydrogeological observations and effective ANN-based forecasting procedures that maximize out-of-sample reconstruction skill while preserving long-period dynamics. The reconstructed and forecast GWL series are intended to update the basin hydrodynamic model and assess changes in the catchment water balance.

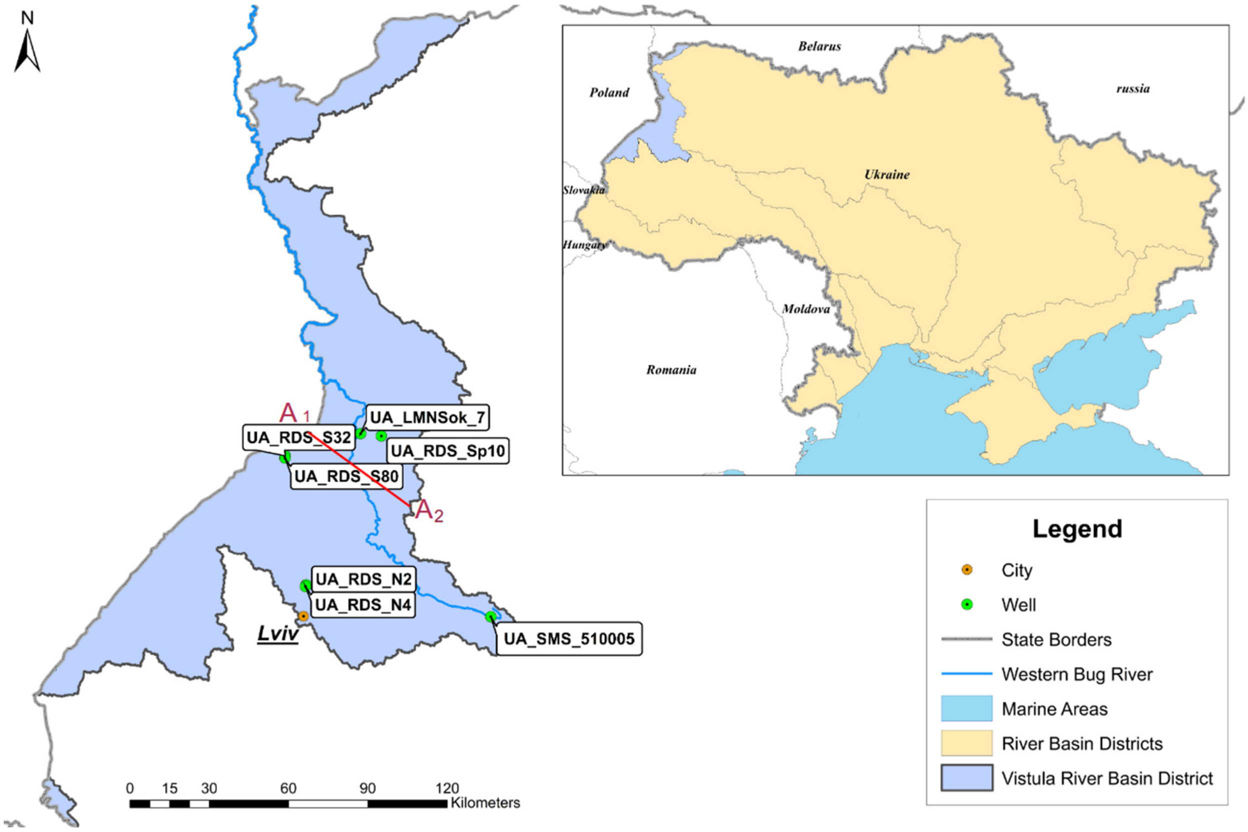

Figure 1. Map of the Vistula River basin in Ukraine, most of which belongs to the Western Bug River basin, with selected observation wells used for groundwater level reconstruction and with hydrogeological section line A_1–A_2 (see Figure 2).

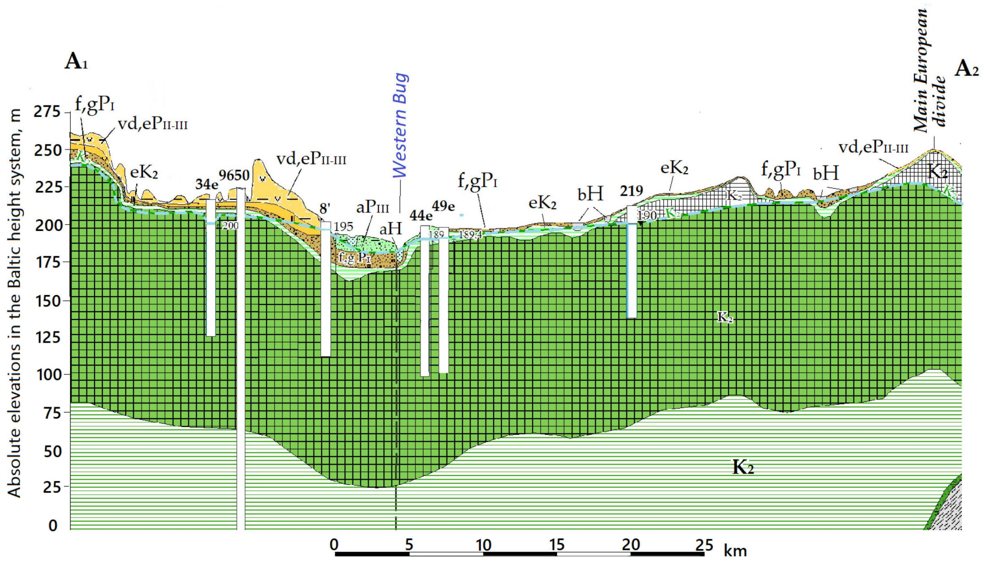

Figure 2. Hydrogeological section along the A_1–A_2 line (see Figure 1).

2. Research Methods and Stages

When long historical groundwater-regime series are available, missing years can be reconstructed using autocorrelation or autoregression, based on correlations between successive elements of the observed time series.

At the first stage, we were reproducing the monthly mean GWL for well No. UA_SMS_510005 (or 51-5a) in the first from the surface combined Quaternary and Upper Cretaceous aquifer complex (Figure 3) with the longest record (1972–2011), located in the upper Western Bug basin (Figure 1). All data were obtained by manual measurements (most likely by different observers), which a priori carries the possibility of errors. To screen unreliable values and identify trends, we applied data-quality testing with the sequential Mann–Kendall (SQMK) criterion. The Mann–Kendall test is a non-parametric method for detecting monotonic trends in time series data. Its sequential form (SQMK) enables the identification of trend changes and anomalous segments over time, which makes it suitable for screening groundwater level observations and isolating long-term trends. During verification of monthly mean GWL for 2000–2011 (the main target period), naturally high values from the 2003 flood were initially treated as outliers and removed, which slightly reduced the annual mean. When the full 1972–2011 record was analyzed, these flood-related values were correctly retained, while true errors were identified and removed (including unreliable first-year observations). Thus, trend reliability improves with longer series, enabling better interpretation of natural anomalies.

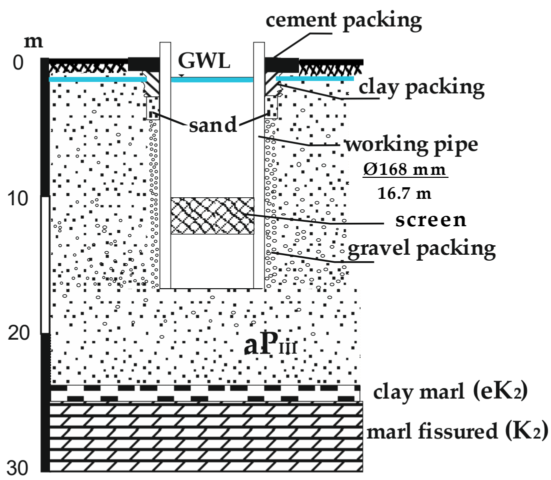

Figure 3. Hydrogeological section and observation well No. UA_SMS_510005 construction.

Groundwater is recharged by atmospheric precipitation, and in river floodplains—also by pressure waters of the second aquifer in the Upper Cretaceous deposits. In a narrow strip (10–30 m) along the river there may also be a flow of river water into groundwater during periods of high level in the river. However, daily and monthly groundwater level fluctuations rarely have a clear and synchronous relationship with the sources of their recharge. This is due to delays in water filtration through unsaturated or poorly permeable soils and rocks, changes in atmospheric pressure, electrostatic field charge, geodynamic phenomena, etc.

The long-term average groundwater levels below the surface, in observation wells (Figure 1), are distributed as follows: UA_LMNSok_7—3.15 m, UA_RDS_N2—1.68 m, UA_SMS_510005—1.1 m, UA_RDS_N4—0.90 m, UA_RDS_S80—0.58 m, UA_RDS_S32—0.55 m, UA_RDS_Sp10—0.24 m.

Long series of average daily or average monthly GWL values for many years can reveal dangerous trends associated with groundwater recharge deficits or excesses. In natural conditions, multi-year trends reverse with alternating wet and dry cycles.

https://doi.org/10.3390/w18172105

At the second stage, we tested simulation modeling with potential regime-forming factors. According to the register of monitoring wells monitored by the State Enterprise "Geoinform of Ukraine" (Kyiv), well No. 51-5a is in an undisturbed regime of groundwater; therefore, the list of regime-forming factors is limited only to natural ones. Multiple correlation analysis across several lags did not show strong relationships between GWL and either monthly precipitation totals or monthly mean air temperature. The highest Pearson coefficient was about 0.51, but this was between the monthly precipitation total and the average monthly temperature. When analyzing the correlation between daily data series for drainage systems, peak associations between precipitation and groundwater levels were identified with a lag of 5 to 18 days, depending on the lithological composition of the aeration zone. However, the coefficient values were again very low—less than 0.15. The slow and vague response of groundwater levels to precipitation, in contrast to the response of surface water levels, significantly complicates the testing of artificial neural network methods and, in this case, limits the use of precipitation amounts for GWL reconstruction (however, for shallow aquifers with strong direct meteorological control, models with exogenous predictors are appropriate and effective).

There are no other sources of groundwater recharge for the studied well (No.51-5a) except for precipitation. Periodic inflow from the confined aquifer (K_2) is possible; however, these waters are ultimately also of infiltration origin.

Therefore, we reconstructed values for 2012–2017 using ANN-based autocorrelation of the corrected GWL series [23]. With the improved series (from 1973 onward), network performance increased from 69.7% to 90%. For one site, RBF architectures (RBF 1-17-1 and RBF 1-21-1) performed best. For objects with stronger trends and cycles, ANNs on multilayer perceptrons (MLP) were used, which have demonstrated their high efficiency in solving similar tasks in previous studies [24]. However, model variants showed substantial uncertainty in level fluctuations, likely due to combined heterogeneous controls and temporal shifts in dominant drivers. Agreement with precipitation was acceptable only during the first four years (to about 2015), suggesting that the predictor-response of GWL relationships changed later.

Artificial neural networks (ANNs) of the multilayer perceptron (MLP) type are supervised machine-learning models designed to approximate complex nonlinear relationships between input and output variables. An MLP consists of an input layer, one or more hidden layers of neurons, and an output layer, with information propagated forward through weighted connections and nonlinear activation functions. During training, the network parameters are iteratively adjusted by minimizing an error function using gradient-based optimization algorithms. Owing to their ability to capture nonlinear dynamics and temporal dependencies through lagged inputs, MLP networks have been widely applied in hydrogeology for modeling groundwater level fluctuations, particularly under conditions of nonlinearity, non-stationarity, and incomplete observations.

The third stage. Wavelet analysis allows simultaneous localization of signal features in both time and frequency domains, making it particularly suitable for non-stationary hydrogeological data. By separating short-term, medium-term, and long-term oscillatory components, this approach enables the isolation of dominant multi-year trends from high-frequency variability, thereby improving the stability and predictive performance of subsequent modeling. To improve accuracy and extend the reliable reconstruction horizon, we applied wavelet analysis [25] to identify periodic components of GWL variability. We also performed Fourier spectral analysis to assess dominant periodicities without explicit temporal localization. Together, these methods supported component-based modeling.

After isolating the most irregular short-period variability, we reproduced monthly mean GWL with MLP models separately for medium- and long-period components; this strategy produced the most stable long-horizon reconstructions. For well 51-5a, we reconstructed the period from June 2011 to 2023 (from the 461st to the 600th value of the series).

For shorter GWL records (about 10 years), we additionally tested ANN modeling with component separation for both monthly and daily mean series. For wells No. 4 (UA_RDS_N4, Figure 1) and No. 10 (UA_RDS_Sp10), the observations cover 2008–2017; the reconstruction was performed until November 2020 and June 2024, respectively.

The following mathematical and statistical software packages were used: Scilab 2025.1.0; Mann_Kendell_Test_Yearly_OutlierRemoval.exe; GNU PSPP 1.6.2-g78a33a; wx-Maxima 22.04.0.; IDL 6.1 (Wavelet analysis). A specialized programming language combined with a graphical interface: R version 4.3.1 (2023-06-16 ucrt) using the EZR package (version 1.68). Code editor: Notepad++ v8.8.8; office suite: LibreOffice 7.5.2.2. Graphics packages: Inkscape 1.0.2 (e86c870879, 2021-01-15, custom), CorelDRAW and GIMP 2.10.38.

3. Results

3.1. Reconstruction for the Full Time Series

Because our main interest is the border zone of the Western Bug basin, we first analyzed wells in the basin's western part. A key limitation was the short record length. For well No. 2 (or UA_RDS_N2, Figure 1), located in the Nedilchynska drainage system, the record spans 6 years (72 monthly means, 2008–2013). For well No. 7 near v. Sokal (UA_LMNSok_7, Figure 1), the record spans 109 months (January 2009 to January 2018). The longer record at well No. 7 revealed a clear approximately 3-year cycle (Figure 4b), whereas for well No. 2 this periodicity was weak (Figure 4a).

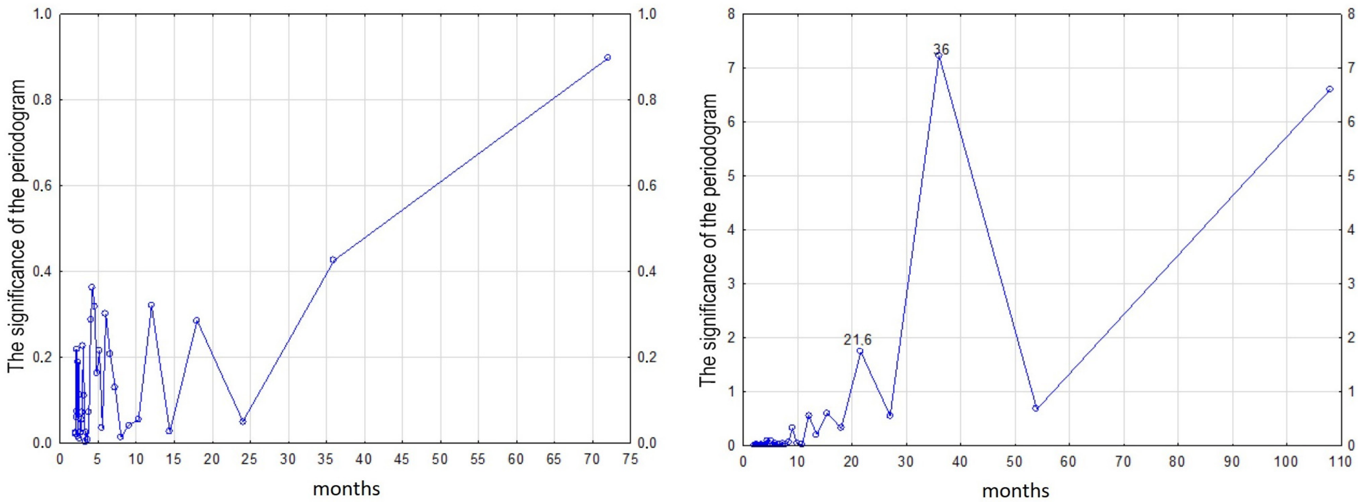

(a) (b)

Figure 4. Fourier spectral analysis for short GWL observation series: (**a**) well No. 2; (**b**) well No. 7.

Because the GWL series for well No. 2 did not show a clear trend or dominant periodicity (Figure 4), RBF networks were selected for ANN training.

For well No. 7, the longer series showed a distinct trend and a pronounced 36-month cycle (Figure 4b), so an MLP-based ANN was applied. Reconstruction accuracy for this well was higher than for well No. 2.

Hydrogeological conditions in the areas are similar and can be characterized by the general section in Figure 2.

Well UA SMS 51-5a (GRANDE-U database; State Geological Service of Ukraine network) was identified as the most representative site for GWL reconstruction. It is located in the upper Western Bug basin, in Ruda-Koltivska village, Zolochiv district, Lviv region (Figure 1). Although observations stopped in 2011, the historical record is long (since 1972), ensuring robust ANN training. The series contains 460 monthly observations with centered variance var(x) = 0.058247. The long-term fluctuation amplitude is about 1.5 m, indicating relative system stability with meaningful variability; total signal energy (Energy time = 0.05812) is also consistent with low-amplitude fluctuations in stable groundwater systems. Fourier spectral analysis revealed a dominant 153-month cycle (12.75 years) (Figure 5), supporting the use of MLP for extrapolation.

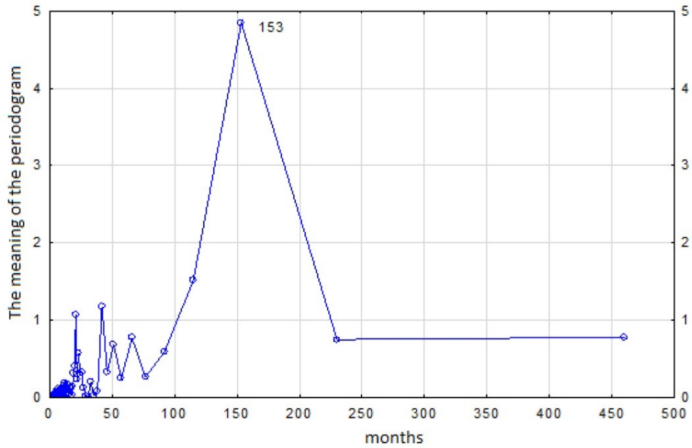

Figure 5. Fourier spectral analysis of the GWL time series in well No. UA SMS 51-5a (460 observed monthly values).

In the MLP notation, the first value is the number of input neurons (153; Table 1), the second is the number of hidden neurons (variable), and the third is the number of output neurons (1). For reliable learning, the training record should be at least as long as the dominant cycle duration (Figure 5).

Table 1. Best MLP architectures used to reconstruct monthly mean GWL in well UA SMS 51-5a using time-series autocorrelation.

N	Architecture	Training Algorithm	Validation Performance	Validation Error	Test Performance	Test Error
1	MLP 153-11-1	BFGS 22	0.662	0.0047	0.903	0.0016
2	MLP 153-17-1	BFGS 24	0.671	0.0044	0.903	0.0016
3	**MLP 153-5-1**	BFGS 34	0.699	0.0036	0.902	0.0016
4	MLP 153-21-1	BFGS 21	0.683	0.0042	0.906	0.0017
5	MLP 153-19-1	BFGS 19	0.676	0.0045	0.903	0.001655
6	**MLP 153-10-1**	BFGS 44	0.670	0.0045	0.892	0.001863

From about 5000 tested MLP variants, six best-performing networks were selected (Table 1). All used sum-of-squares loss and logistic activation in hidden neurons. Training performance ranged from 0.911 to 0.932; training error ranged from 0.0004 (MLP 153-10-1) to 0.0012 (MLP 153-19-1). Output activation was identical in four models; in MLP 153-5-1 and MLP 153-10-1, it was logistic (Table 1). The data are subject to a sequential chronological distribution. Data partitioning included 153 months for training (which is one full dominant cycle), 307 months for a long-horizon out-of-sample evaluation period, and 73 months for testing (reconstruction).

The MLP 153-5-1 and MLP 153-10-1 ANN models (Figure 6), both with logistic output activation and high learning performance, reproduced observed level changes most realistically (including consistency with precipitation patterns and independent level data from observation wells tapping the same aquifer under similar conditions; see Figure S2).

Despite this overall agreement, systematic differences in bias are evident between the two models. The MLP 153-5-1 configuration tends to slightly increase high-water phases, reflecting a stronger sensitivity to cumulative recharge signals. In contrast, the MLP 153-10-1 model exhibits a lowering of peak levels and a smoother representation of minima.

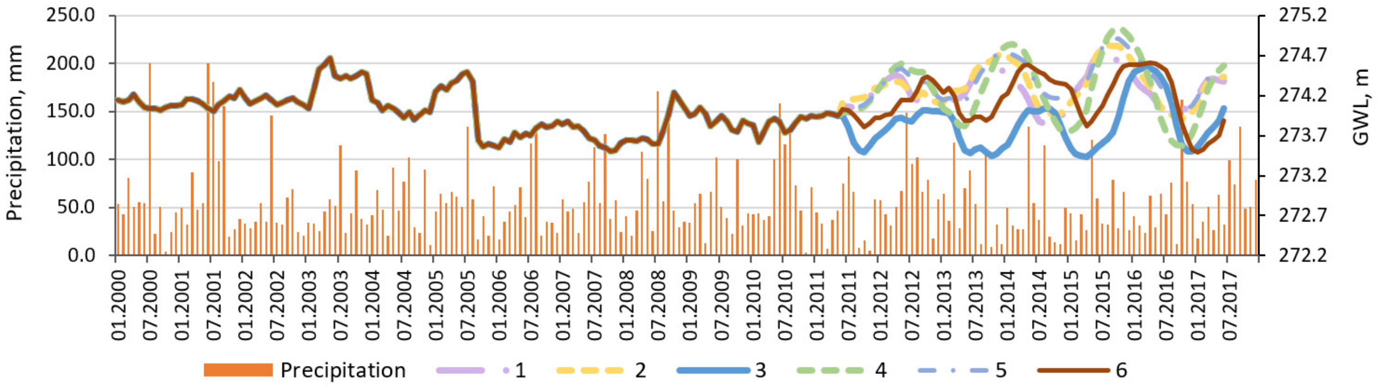

Figure 6. Observed (to 1 June 2011) and reconstructed monthly mean groundwater levels for well UA SMS 51-5a (Ruda-Koltivska village, upper Western Bug basin): 1—MLP 153-11-1; 2—MLP 153-17-1; 3—MLP 153-5-1; 4—MLP 153-21-1; 5—MLP 153-19-1; 6—to 1 June 2011—the observed groundwater-level series, after—MLP 153-10-1.

Importantly, both models retain a similar temporal structure of groundwater level variability, implying that the observed bias primarily affects absolute level estimates rather than the reproduction of underlying dynamics. Consequently, either model may be used for groundwater level reconstruction following appropriate bias adjustment, depending on whether amplitude fidelity or stability of long-term trends is prioritized.

Reconstruction of GWL using the full series gave $R^2 = -0.07$, indicating that the model performed worse than a simple mean baseline. Although MAE = 0.12 m appears small, the total GWL amplitude is only 1.58 m (274.67–273.09), so the relative error is substantial (about 7.6% of the range). This result confirms that point-error metrics alone can be misleading when variance is low; skill should be interpreted jointly with baseline-relative measures and phase-amplitude fidelity. Full-series MLP learning likely fails because:

- The model must compromise between reproducing short-term variability and the dominant low-frequency trend.
- Short-term fluctuations interfere with learning long-period structure.
- Regularization (L2 = 0.1), while useful for generalization, suppresses weights and can reduce the ability to capture long cycles.
- During validation, noise from short-term fluctuations triggers early stopping and limits effective learning.

To improve data reconstruction and isolate dominant trends, we decomposed the GWL series into temporal components using wavelet analysis.

3.2. Reconstruction with Component Separation

Different-period components of GWL variability were identified using a continuous Morlet wavelet transform (Figure 7) applied to 460 average monthly values (~38.3 years). The statistical significance of periodicities was assessed using Monte Carlo testing.

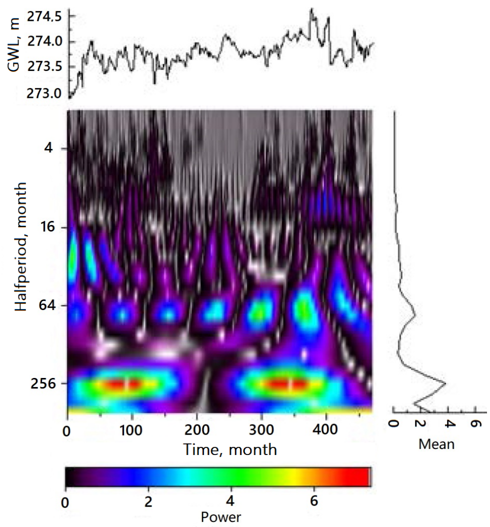

Figure 7. Gaussian wavelet periodogram of GWL values for well No. UA SMS 51-5a (1972–2011). Top: chronological series of observed monthly means; right: average long-term cycle intensity.

Wavelet settings were: shape parameter w0 = 6 (balanced time-frequency localization); number of scales = 126; resolution = 0.0625; initial scale s0 = 2Dt; reconstruction constant Cdelta = 0.776; and FFT-based computation (nfft = 512).

Wavelet analysis identified periodicities with different hydrological significance:

- Short-period fluctuations (<12 months), mainly reflecting immediate weather forcing, behaved as high-frequency noise and were weak in the periodogram for this well.
- Medium-period fluctuations (13–48 months), related to seasonal to interannual climate variability, appeared as weak rhythms with a characteristic period of about 1.8 years (Figure 7).
- Long-period fluctuations (≥48 months) were most clearly expressed by an approximately 11.5-year cycle (consistent with solar cyclicity). A weaker feature near ~5 years was also present. The highest-energy spots in the lower periodogram corresponded to a very long cycle of about 42–43 years.

Morlet and Monte Carlo scalograms (Figure 8) show similar structures, with high energy around ~11 years and at >~38 years. Only the ~11-year band lies clearly within the 95% confidence region. Overall, the strongest energy is concentrated in the 100–150 and >420 month ranges, i.e., in medium- and long-period variability.

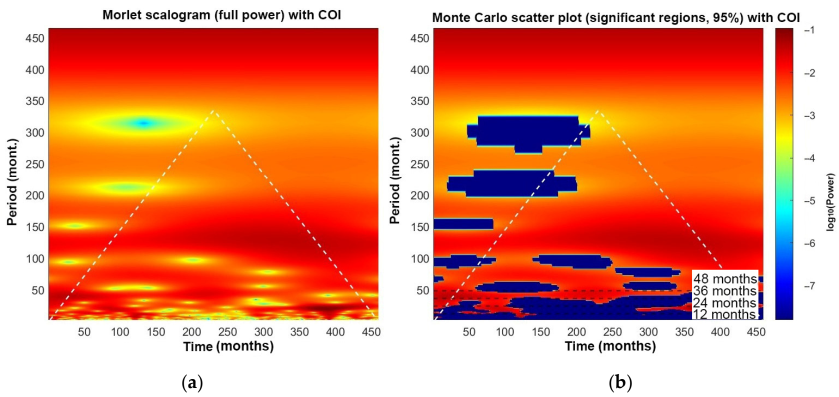

Figure 8. Morlet (**a**) and Monte-Carlo (**b**) scalograms with confidence interval (COI). Within the triangle bounded by the white dashed line—closer to the center and at shorter periods (along the vertical axis)—the results are most reliable, as they are not subject to edge effects.

3.3. Component Analysis (Period-Based Decomposition)

Figure 9a presents wavelet-derived components of the GWL series. The short-period component (<12 months) has high frequency and narrow spikes. The medium-period component (12–48 months) reflects interannual 2–4-year rhythms. The long-period component represents slow multi-year oscillations (about 7–11 years). Medium- and long-period components carry the main regime information.

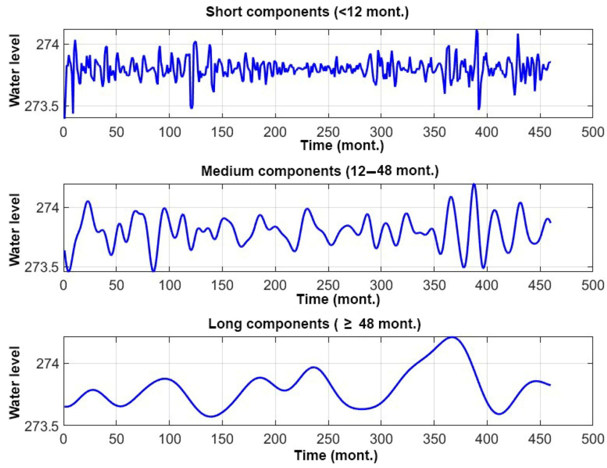

(**a**)

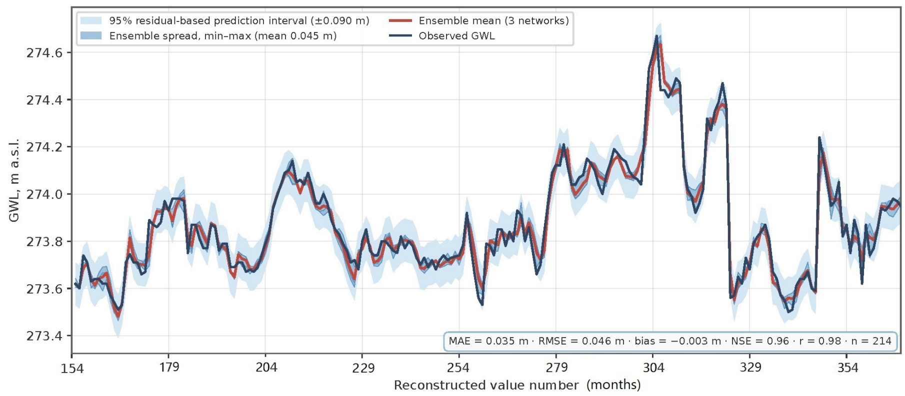

(**b**)

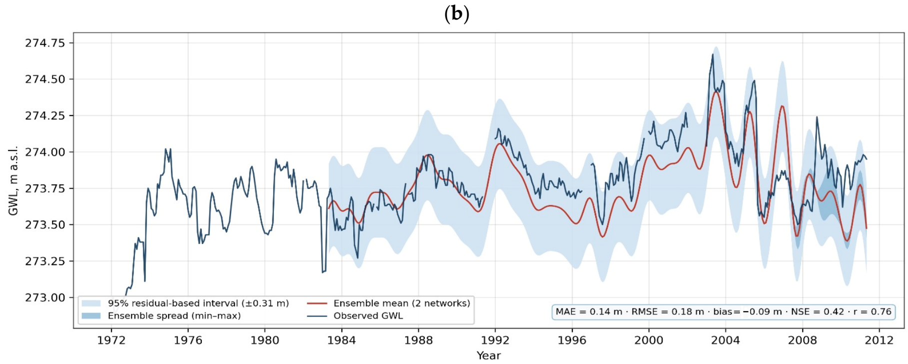

(**c**)

Figure 9. Wavelet component composition of the GWL signal (460 monthly mean values), (**a**) and reconstructed groundwater level values in well UA SMS 51-5a (**b**,**c**), (**b**)—with an uncertainty band derived from an ensemble of the three best MLP networks (153-21-1, 153-19-1, 153-10-1; n = 214). The ensemble spread (min–max) and the 95% reconstruction interval based on residuals (±0.090 m) are shown; (**c**) based on an ensemble of the two best MLP networks (136-24-1 and 136-37-1) for the test "reconstruction" period of 1983–2011. The spread of values within the ensemble (minimum–maximum) and the 95% prediction interval (±0.31 m), determined based on residuals, are shown.

Short-period variability accounts for about 14% of the total energy, medium-period for about 31%, and long-period for about 45%. Thus, long-period structure dominates groundwater-level variability and likely reflects climate-scale controls. The total explained energy of the three components is about 89.6%; the remainder is residual variability. The decomposition is numerically consistent (summation error ~1×10^{-16}), and the reconstructed total series agrees well with observed data (R~0.95).

Therefore, GWL dynamics in this well are governed by a combination of long-term trends and interannual cycles, suggesting sensitivity to large-scale climatic and thermobaric variability (including North Atlantic and solar-related signals).

Figure 9b shows the reconstruction of the GWL using the "one-step-ahead" algorithm: the network received 153 actual preceding months and predicted the next one (a total of 214 reproduced values). A high correlation (Table 2) reflects the smoothness of the series itself, rather than the method's ability to reproduce it. A correlation coefficient of 0.76 was obtained after solving a more complex problem—reconstructing the level from two decomposed components (Figure 9c)—and precisely for this reason, the coefficient is lower, yet at the same time, it is more reliable.

Table 2. GWL reconstruction accuracy metrics for well UA SMS 51-5a for individual MLP networks and their ensembles (n = 214 and 310 observations).

Architecture of Chain	MAE, m	RMSE, m	Bias, m	NSE	r
MLP 153-21-1	0.045	0.058	−0.003	0.94	0.968
MLP 153-19-1	0.045	0.059	−0.003	0.93	0.966
MLP 153-10-1	0.026	0.034	−0.002	0.98	0.989
Ensemble average	0.035	0.046	−0.003	0.96	0.980
MLP 136-24-1	0.154	0.192	−0.094	0.33	0.731
MLP 136-37-1	0.138	0.173	−0.077	0.46	0.766
Ensemble average	0.145	0.180	−0.086	0.42	0.757

Table 2 presents statistical accuracy metrics for various networks and the average accuracy of the ensemble (MAE, RMSE, systematic bias, NSE; correlation coefficient).

The isolated medium-period component exhibits smooth, quasi-periodic oscillations with an amplitude of approximately 0.5 m. ANN training used scaled conjugate gradient, gradient descent, and quasi-Newton optimizers. Identity activation was used in hidden and output layers, with sum-of-squares loss. Performance was near 1 for training and testing, with validation performance 0.99340; errors were on the order of 1×10^{-11}. These near-perfect values indicate that the decomposed component is highly learnable in this setup, but they should not be interpreted as universal generalization performance for other wells or future hydroclimatic regimes.

Figure 10a shows training (48 points) and validation (412 points) up to the 460th monthly value (2011), followed by reconstruction to the 600th value (2023). Thus, major GWL fluctuations were reconstructed for 142 months (~11.8 years).

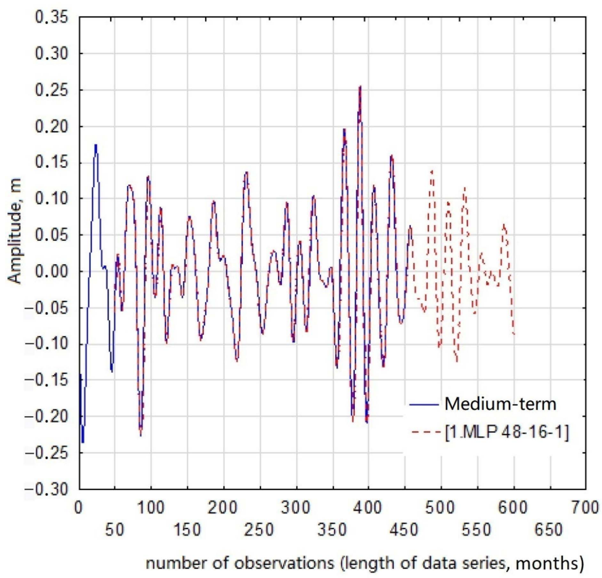

(**a**)

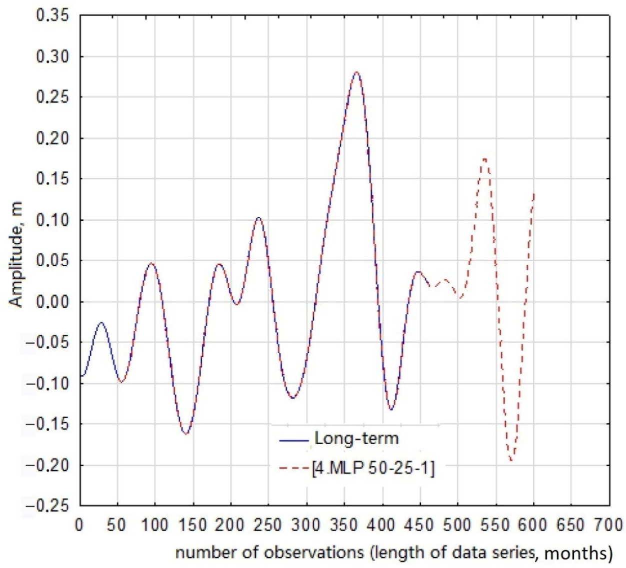

(**b**)

Figure 10. Observed and reconstructed monthly mean GWL components in well UA SMS 51-5a: (**a**) medium-period component using (MLP 48-16-1); (**b**) long-period component (MLP 50-25-1), relative units.

3.4. Reconstruction of Long-Period Fluctuations

As in Figure 10a, long-period modeling included training/validation on 460 observed monthly values and reconstruction up to the 600th value (about 140 reconstructed months, to 2023) (Figure 10b). The activation functions and loss were the same as for the medium-period model. Training and validation performance were 0.998, and test performance was 0.996 (additional model characteristics are presented in Table 3). Across model variants, oscillations were nearly synchronous with similar amplitudes and small differences in extrema. This confirms that the long-period component is the most stable basis for long-horizon reconstruction (up to ~144 months). For operational use, however, this deterministic simulation should be supplemented by uncertainty ranges (e.g., ensemble spread or residual-based reconstruction intervals) (see Figure 9b, Table 2).

Table 3. Characteristics of the best MLP networks used to reconstruct GWL values from long-period component fluctuations.

N	Architecture	Training Algorithm	Training Error	Validation Error	Test Error
1	MLP 50-20-1	BFGS 7220	3.650×10^{-13}	4.9821×10^{-13}	3.3714×10^{-13}
2	MLP 50-2-1	BFGS 9999	2.0282×10^{-14}	2.7576×10^{-14}	1.6389×10^{-14}
3	MLP 50-2-1	BFGS 9999	2.5135×10^{-14}	3.4249×10^{-14}	2.0642×10^{-14}
4	MLP 50-25-1	BFGS 10000	4.0049×10^{-13}	5.5654×10^{-13}	3.6485×10^{-13}
5	MLP 50-20-1	BFGS 1190	3.6917×10^{-13}	4.4914×10^{-13}	3.5454×10^{-13}

Using the MLP 50-25-1 curve (Figure 10b), together with interpolation and proportionality criteria, we obtained realistic reconstructed GWL values (Table 4).

Table 4. Selected reconstructed GWL values for well UA SMS 51-5a (2014–2022).

Model-Derived Characteristics			Observed Analog			Accepted Reconstructed GWL (m)
Date	**Model Relative Value (y-Axis)**	**Model Index (x-Axis)**	**Observed Index (x-Axis)**	**Observed GWL (m)**	**Long-Period Component (m)**	
December 2014	0.0054	503	435 436	273.97 273.82	273.973 273.828	273.91
August 2017	0.175	535	341	274.04	274.215	274.04
November 2018	0.0455	550	249 250	273.85 273.83	273.902 273.875	273.84
February 2019	−0.0035	553	394 395	273.56 273.62	273.567 273.613	273.60
August 2020	−0.194	571	-	-	-	273.21
February 2022	0.004	589	394 395	273.56 273.62	273.567 273.613	273.58

It turned out that the direction of the trend during the final stage of training is of great importance. If this trend is downward, the trend derived from extrapolated values may prove to be slightly lower than the actual one, as evidenced by testing the method (see Figure S3).

To quantify the roles of components in full-series variability and their relationships with meteorological forcing, we computed multiple correlations among observed GWL, three wavelet components, monthly precipitation totals, and monthly mean air temperature. Correlation analysis using both Pearson's parametric and Spearman's nonparametric coefficients indicates that medium- and long-period components of GWL variability exhibit substantially stronger associations with the overall fluctuations of the complete time series than the short-period component. Specifically, Pearson correlation coefficients of approximately 0.68 were obtained for both medium- and long-period components, while Spearman coefficients reached 0.66 for the medium-period and 0.71 for the long-period component. In contrast, short-period fluctuations show weaker correspondence with the total GWL variability but display the strongest correlation with air temperature, exceeding that of the complete observed series. None of the extracted components exhibits a statistically significant correlation with precipitation, consistent with the behavior observed for the full GWL time series. These results support the modeling choice to prioritize medium- and long-period components for ANN to treat short-period variability as limited-skill noise for long-horizon projections.

To validate the proposed data reconstruction framework, we applied the same component-based procedure to two additional wells (on Nedilchynska and Spasivska drainage systems) with shorter records. Initial quality control used Mann–Kendall testing (Figure 11), and unreliable points were removed. Combined, the two series contained 3653 daily shallow-groundwater observations for 2008–2017.

Because the long-period component has the greatest contribution to observed GWL variability, reconstruction for wells No. 4 (Nedilchynska) and No. 10 (Spasivska) (Figure 12) was performed primarily for this component.

We first analyzed monthly data. For each well, the input series consisted of 120 values (2008–2017). Wavelet decomposition identified three components with different periodicities.

Component contributions for well No. 4 were: short-period 35.21%, medium-period 29.30%, and long-period 14.89% (total 79.41%).

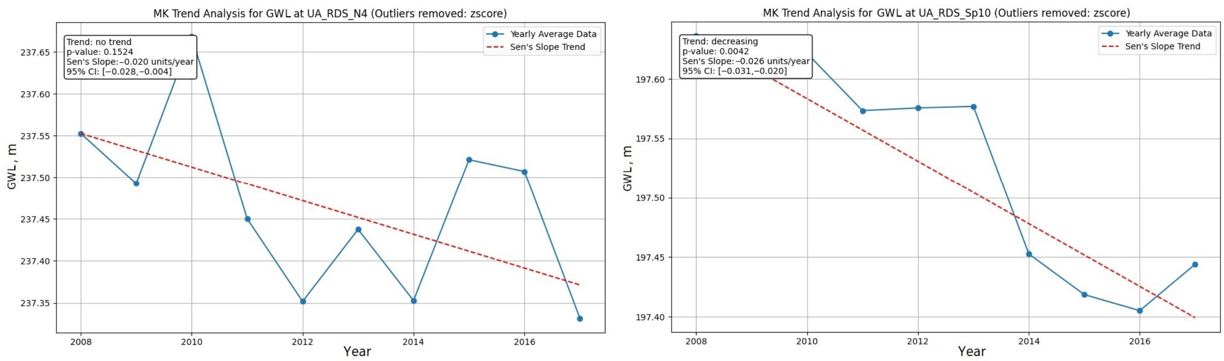

(**a**) (**b**)

Figure 11. Trends in measured GWL in selected wells in the Nedilchynska (**a**) and Spasivska (**b**) drainage systems, 2008–2017.

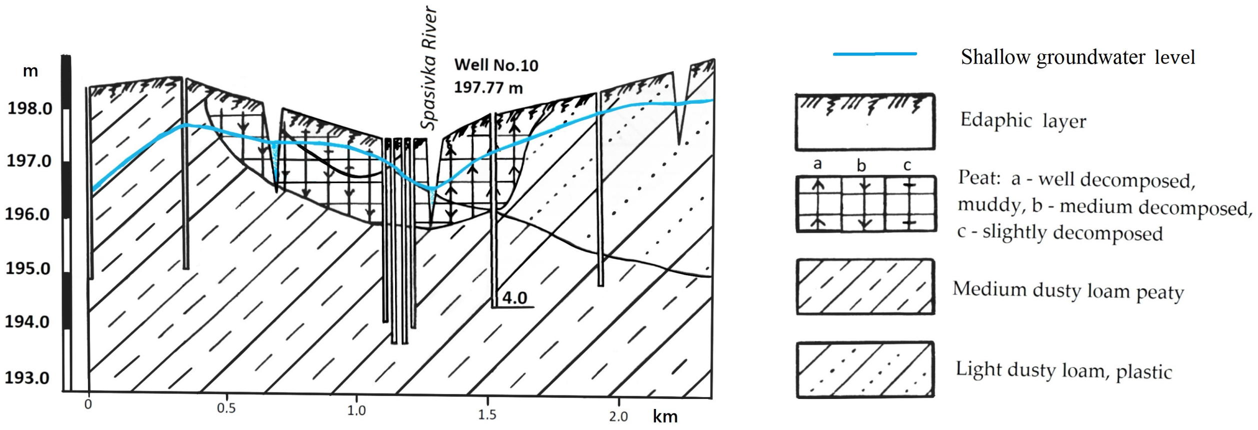

Figure 12. Hydrogeological section through the well site, in which well No. 10 is located and the absolute surface mark at the point of its mouth.

Component contributions for well No. 10 were: short-period 50.87%, medium-period 14.61%, and long-period 14.25% (total 79.72%).

Monte Carlo wavelet scalograms for the 10-year monthly series of wells Nos. 4 and 10 show dominant 12-month energy (especially in well No. 10; Figure 13b). Unlike well UA SMS 51-5a, this pattern is typical of shallow unconfined groundwater in the first aquifer from the surface.

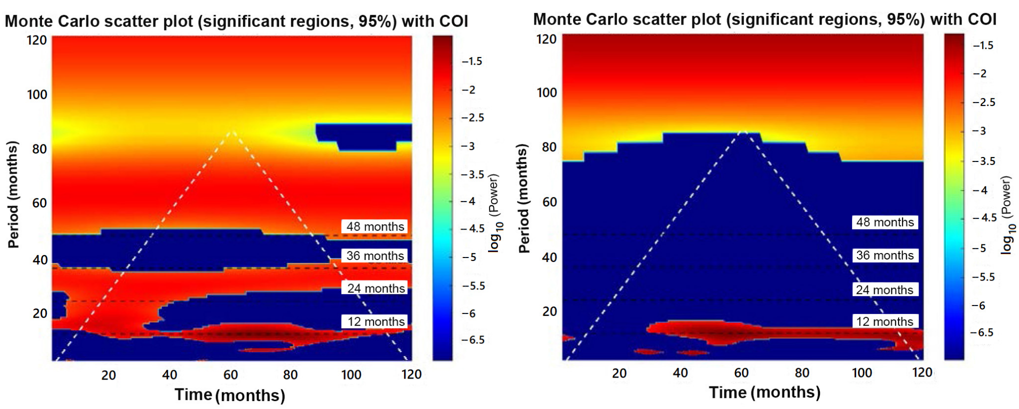

(**a**) (**b**)

Figure 13. Monte Carlo wavelet scalograms with significant regions for observed GWL series: (**a**) well No. 4; (**b**) well No. 10. The white dashed line is the same as in Figure 8.

However, after isolating long-period components, only one full minimum and two maxima were available in each well (Figures 14a and 15). This is insufficient for reliable ANN reconstruction using the same approach as for records longer than 30 years. Consequently, the RMSE value turned out to be slightly higher (Table 5) than in the previous case (Table 2).

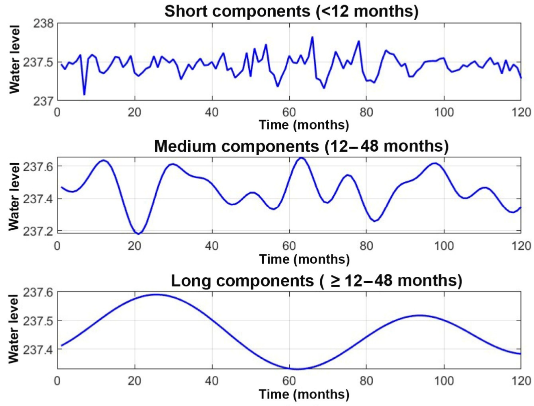

(**a**)

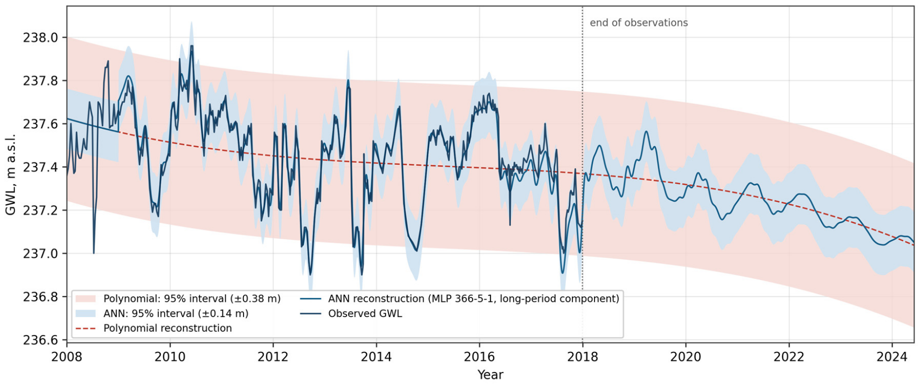

(**b**)

Figure 14. Separation of different-period components based on monthly mean GWL values for well No. 4 (Nedilchynska drainage system) (**a**) and reconstructed GWL in well No. 4 with uncertainty bands (**b**) (residual-based, 95% prediction interval derived from residuals of 3653 daily observations from 2008 to 2017): ±0.38 m for polynomial reconstruction and ±0.14 m for reconstruction using the long-period component via an artificial neural network. The bands cover the entire reconstructed series, including the extrapolation period following the conclusion of observations.

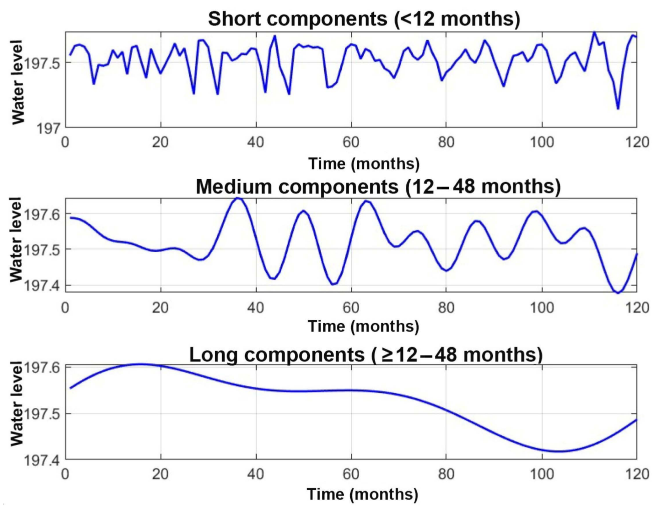

Figure 15. Separation of different-period components based on monthly mean GWL values for well No. 10 (Spasivska drainage system).

Table 5. Metrics for the accuracy of groundwater level (GWL) reproduction for well No. 4 (3653 daily observations, 2008–2017).

Reconstruction Method	MAE, m	RMSE, m	Bias, m	NSE	r
Polynomial	0.156	0.194	−0.000	0.10	0.32
ANN 366-5-1 (long component)	0.043	0.071	−0.002	0.88	0.94

Component plots also show decreasing fluctuation amplitude as period length increases.

ANN experiments indicated that monthly discretization was insufficiently accurate for these wells. Therefore, we repeated the analysis using daily data (Figure 16, green curve; Figure 17, green and pink curves).

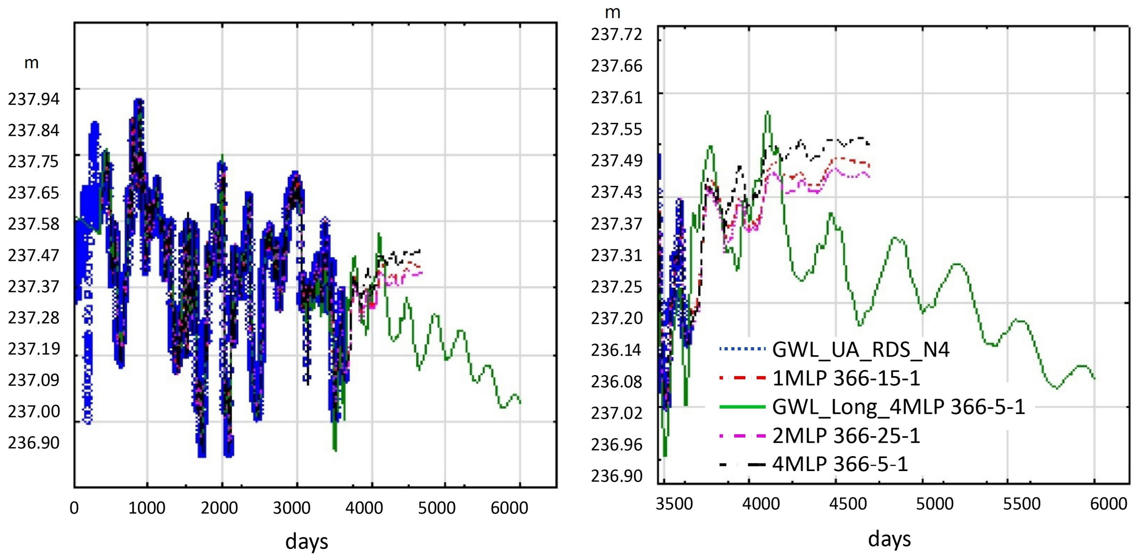

(**a**) (**b**)

Figure 16. Polynomial reconstruction of the long-period GWL component for well No. 4 (Nedilchynska drainage system) to June 2024: (**a**) 6000 days from 1 January 2008; (**b**) observed data are available through day 3653—31 December 2017.

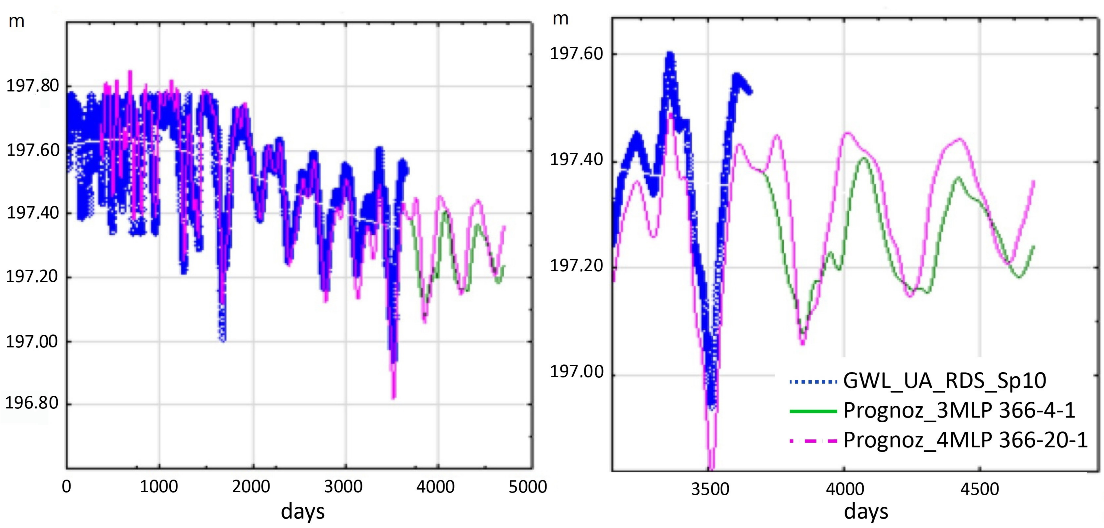

(**a**) (**b**)

Figure 17. Reconstruction of absolute GWL values by polynomial approximation of the long-period GWL component for well No. UA_RDS_Sp10 (Spasivska drainage system): (**a**) to November 2020 (4700 days from 1 January 2008); (**b**) observed data are available through day 3653.

The first iteration reproduced shallow-groundwater fluctuations through day 4700 (November 2020) (Figure 17). The reconstructed dynamics were consistent with regional low-water conditions and an approximately 11-year solar cycle (2009–2020), with high activity in 2014–2015 and a minimum around August 2019. The period from 2015 to 2019 was characterized by below-average precipitation and a pronounced recession of shallow groundwater levels. The obtained values, together with the previous actual ones, were used for machine learning and further reproduction of GWL data in well No. 10 up to the 6000th value (Table 6). For the following period (November 2020–June 2024), the same model projects trend recovery (Figure 18), consistent with increased precipitation. The long-term trajectory in Figure 17a resembles alternating 11-year cycles. In contrast, the modeled behavior for well No. 4 (Figure 16) appears less realistic because it continues to decline after day 4700.

Table 6. Accuracy metrics for groundwater level (GWL) reconstruction for well No. 10 (3653 daily observations, 2008–2017).

Reconstruction Method	MAE, m	RMSE, m	Bias, m	NSE	r
Polynomial	0.110	0.134	+0.000	0.34	0.58
ANN MLP 366-4-1	0.052	0.067	−0.011	0.83	0.95
ANN MLP 366-20-1	0.052	0.067	−0.011	0.83	0.95

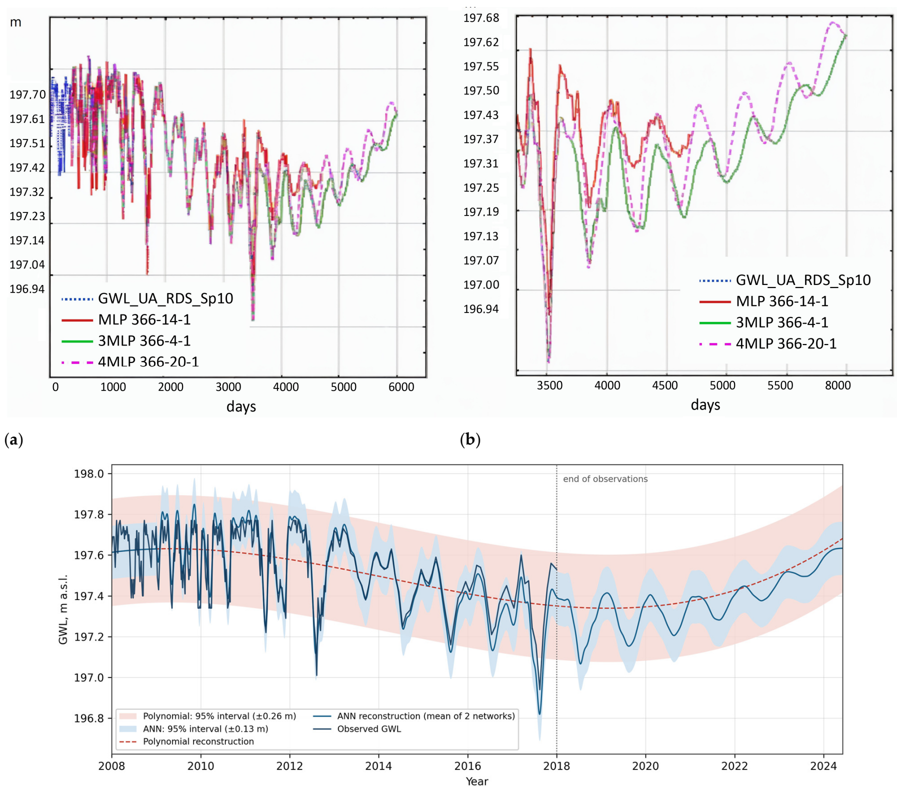

Figure 18. Observed and reconstructed GWL values in well No. UA_RDS_Sp10 (m, absolute elevation): (**a**) full series, (**b**) enlarged reconstructed segment (values 3654–6000), based on polynomial approximation and ANN-modeled long-period fluctuations; reconstructed groundwater level values (**c**), shown with uncertainty bands (residual-based, 95% prediction interval calculated from residuals based on 3653 daily observations from 2008 to 2017): ±0.26 m for polynomial reconstruction and ±0.13 m for ANN reconstruction. The bands cover the entire reconstructed series, including the extrapolation period following the end of the observation record.

Later, we found some actual data: the GWL measurements for well No. 10 for the reconstruction years of 2018 and 2019. These data were not used at any stage, providing an independent check. It can be seen (Figure 19a) that the simulated MLP curve (GWLcalc) reproduces the actual fluctuations (GWLobs) quite well, albeit with a constant offset of −9.6 cm (MAE = 0.096 m), which is larger at the edge sections. This may be explained by the fact that we used only long-term fluctuations for the reconstruction, which account for approximately 75–78 percent of the total and short-period fluctuations and absolute displacement were deliberately not modeled. Therefore, a displacement correction is required to reproduce the absolute levels (Figure 19b); after its application, the residual error (RMSE) is only ~0.024 m. It seems that each variant of the MLP model has its own deviation from the actual values. If further studies can prove that such a difference is systematic, we will be able to reproduce with sufficient accuracy not only the nature of the fluctuations and general trends, but also the values of the GWL themselves.

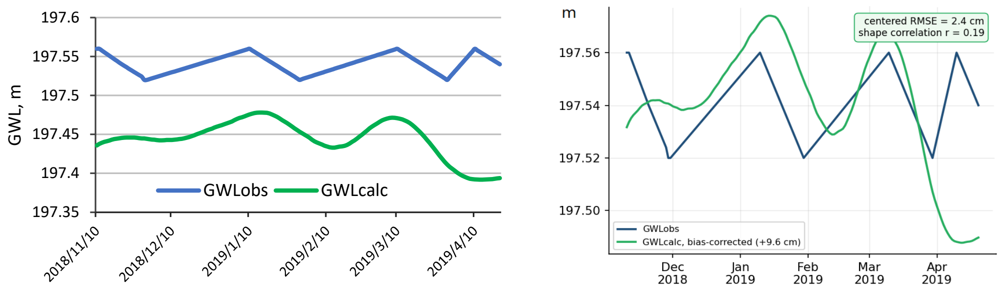

(**a**) (**b**)

Figure 19. The curve constructed from individual actual observation data using interpolation (GWLobs) and the calculated curve (GWLcalc) based on daily values in the MLP 366-14-1 projection, as part of the overall model (see Figure 18) in the range of values from 3967 to 4128 (**a**) and the same after removing the constant offset (bias = −9.6 cm) (**b**).

4. Discussion

The study region in Ukraine is characterized by a significant interconnection between groundwater and the artesian waters found in Upper Cretaceous deposits. In some areas, the latter even reach the surface, yet they remain under pressure due to the presence of a clayey weathering crust. In our view, these features are the primary reasons for the weak correlation between GWL fluctuations and the amount of atmospheric precipitation. The weak coupling between meteorological variables and GWL may be attributed, in part, to seasonal freezing of the near-surface zone, during which groundwater recharge is limited or absent despite precipitation inputs, thereby distorting direct correlations. Therefore, the use of the autocorrelation method employing artificial neural networks proved to be practically the only acceptable option for data reconstruction under such conditions. The worst part is that the absence of clear and significant predictors hinders the development of measures to mitigate the effects of hydrological drought.

In the first case, concerning the groundwater level series for well No. 51-5a, the ANN training was mainly based on data up to 1986, while the period from 1989 to 2020 reflects the regularities of the level regime formation due to the dominance of other regime-forming factors [26], which may reduce the reliability of extrapolation. This likely explains why modeled GWL tracks precipitation reasonably well through about 2015 (the first pan-European hydrological drought) but not in later years. Thus, full-series autocorrelation without frequency-based component separation may be unreliable beyond about 3–4 years.

The wavelet periodogram does not show strong annual cyclicity typical of shallow unconfined aquifers. The identified combination of dominant multi-year cycles and the absence of pronounced annual rhythms associated with external meteorological forcing indicates that groundwater levels in well No. UA SMS 51-5a are controlled by a complex, semi-confined aquifer system. This system is primarily hosted in fractured Upper Cretaceous marls and is hydraulically connected to the overlying Quaternary deposits, resulting in a mixed pressure–recharge regime. The strong low-frequency energy near ~42 years is also consistent with deeper, better-protected horizons [27].

The contribution of different components to long-term GWL dynamics depends strongly on series length and sampling interval. For one well (2008–2013), we compared daily data (2192 values) and monthly means (72 values). Using the same Matlab 2022 workflow, daily data yielded component energies of 0.26% (short), 7.53% (medium), and 88.66% (long), totaling 96.45%. Monthly means produced an opposite distribution: 66.92% (short), 18.71% (medium), and 1.08% (long), totaling 86.71%. This indicates higher uncertainty in component partitioning when only monthly averages are available for short records. The same script and parameter settings were used for both analyses; only the input data source differed.

The highest percentage of the short-period component (50.87%) characterizes the area with the shallowest average GWL (0.24 m). As the water level deepens, the role of this component predictably decreases. The short-period component exhibits the highest correlation coefficients with air temperature. It follows that differentiating groundwater levels across the area based on the proportion of the short-period component can help determine groundwater vulnerability or resilience to drought. As for the other two components, no clear relationship with the GWL depth was found. This issue requires further in-depth study; resolving it will help determine the optimal combinations of fluctuations for data reconstruction, as well as the conditions under which the groundwater regime is most resilient to climate change.

With daily observations (N = 2192, about 6 years), oscillatory structure is visible from 2 days to >4000 days; short components (<365 days) are well resolved, while long components (≥1460 days) dominate total variance.

With monthly averages (N = 72, about 6 years), only 2–144 month scales are represented; intra-month variability is lost, amplitudes are damped, and long components (≥48 months) are poorly resolved because only about 1.5 full 48-month cycles are present.

Therefore, both record length and sampling frequency strongly affect wavelet-based component analysis. For long records, however, monthly averaging can still be useful because it suppresses high-frequency noise and highlights season-to-multiannual rhythms.

Inverse wavelet transform with proper scaling produced a reconstructed series that closely matches observations (Figure 20), with a correlation of about 0.95. RMSE is low, and the reconstruction/original energy ratio is 0.90, indicating that the model captures the main structure of the signal.

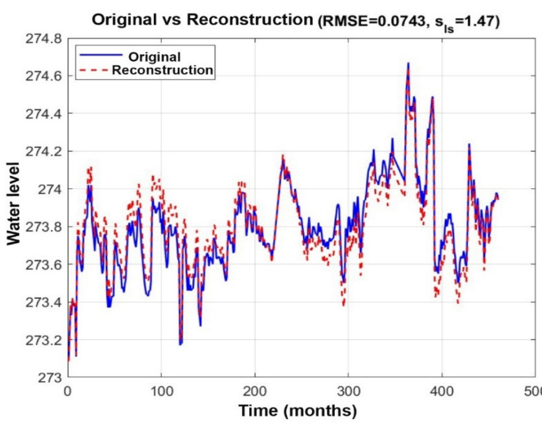

Figure 20. Reconstruction of GWL observations. Blue line: observed GWL; red line: wavelet reconstructed series; sls = 1.47 is the scaling factor.

In terms of MAE and RMSE (Table 2), the best results were achieved using the "one-step-ahead" (t + 1 month) method (Figure 9), where the network utilized data from the preceding 153 months to reconstruct the next month. However, the correlation coefficient of r = 0.98 reflected the smoothness of the data rather than the method's actual effectiveness. Reconstructing the level based on decomposed components is a more challenging task—yielding an r-value of 0.76 for MLP models with 136-24-1 and 136-37-1 configurations—yet this specific metric characterizes the network's true data reconstruction capability.

Observed GWL shows multi-year amplitude around 1.5 m and annual amplitude around 0.5 m; the reconstruction reproduces both well. Before about 1989 (around index 200), modeled values are slightly higher than observed; between indices 200 and 240 (~1993), curves nearly coincide; afterward, minima are somewhat over-smoothed, and some maxima are underestimated. The model reliably captures medium- and long-term groundwater level variations but tends to smooth small-amplitude peaks. This may result from data aggregation, training regularization, and the limited ability of autocorrelation-based neural networks to reproduce short-term, localized recharge responses, in addition to potential measurement uncertainties.

The best long-period projections were obtained with MLP 50-20-1 and MLP 50-25-1 (see Figure 10b). Both show a decline of the long-term amplitude trend after 2003 (month 360 from 1973), consistent with the groundwater table (GWT) behavior of the nearby region. The long-term minimum (the largest negative amplitude) occurs around month 570 (the second half of 2020), followed by a recovery. This is when the 11-year solar cycle of high activity, which caused drought, ended in September, and a cycle of low activity began, contributing to increased water content and the restoration of the GWT after the recession [27,28].

Limitations associated with autocorrelation and the wavelet decomposition of groundwater level (GWL) components arise from the fact that if unprecedented short-term rises or drops in the water level occur during the reconstruction period, the models cannot clearly reproduce them (see Figure S3). While wavelet decomposition allows for the isolation of the long-term component of GWL fluctuations—yielding oscillations with significant amplitude—it is difficult to determine the specific water level for a particular date based on these components alone. Nevertheless, we managed to extrapolate sufficiently accurate values (see Table 4) using the decomposition method.

Recent studies [4] reported the strongest agreement between satellite estimates and groundwater-storage changes in aquifers with rapid water exchange. This supports potential use of the short-period GWL component identified here for GRACE/GRACE-FO validation. Medium- and long-period components can be used to model shallow groundwater level (GWL) based on groundwater levels of the second aquifer from the surface in Upper Cretaceous deposits (GWL_2), where observations are more abundant. In our case, the levels in nearby wells in the first and second aquifers show high pairwise correlation (r = 0.83). The strong coupling between groundwater levels in both aquifers provides a basis for interpreting satellite-derived water storage signals and assessing regional groundwater resource changes. This can be achieved by identifying spatial relationships between hydraulic heads and analyzing the temporal synchronization of their fluctuations. Given known GWL_2 values, the GWL trajectory can be reconstructed retrospectively, and common GWL-GWL_2 fluctuation modes can be identified. From an AI perspective, this cross-aquifer consistency is a useful external plausibility check, although it is not a substitute for independent out-of-sample validation.

We also do not rule out the possibility of using the median instead of a polynomial when reconstructing GWL data. In certain cases—specifically for short time series—this approach proved superior.

The moderate reconstruction performance obtained in this study should be interpreted in light of the noisy and highly variable character of short-term groundwater-level dynamics. Similar behavior was reported by Samalavičius et al. [18], who found that groundwater-level reconstruction was most accurate in wells with relatively smooth dynamics and deteriorated in wells affected by abrupt drawdowns and pronounced short-timescale variability. High-frequency fluctuations may weaken the correspondence between groundwater levels and external environmental predictors, thereby limiting the amount of recoverable signal. This interpretation is also consistent with Bo et al. [29], who demonstrated that filtering short-term groundwater-level fluctuations improved model stability and long-term prediction accuracy. A complementary methodological perspective is provided by Eslamifar et al. [17], who obtained reliable groundwater-storage forecasts by training a multilayer perceptron on structured simulation data generated by a validated system-dynamics model. Their results illustrate the advantages of physically organized training information under data scarcity, although they are not directly comparable with the reconstruction of noisy, point-scale groundwater-level observations.

Bikše et al. [7] reported median NSE values of 0.58–0.76 for 24–63-day gaps, with substantially higher accuracy for shorter gaps. Eslamifar et al. [17] also showed that multilayer perceptron models can support groundwater storage forecasting when combined with system-dynamics simulation data, achieving a training RMSLE of 0.031 and R^2 of 0.77, with testing results of RMSLE = 0.036 and R^2 = 0.71. This highlights the broader usefulness of ANN-based methods in data-limited groundwater applications. In the Baltic Region, Samalavičius et al. [18] further demonstrated the relevance of AI-based approaches for karst groundwater and sinkhole-risk analysis in the Lithuania-Latvia transboundary area (CV R^2 = 0.44–0.79; MAE = 0.12–0.40 m).

Further work may focus on extending the proposed hybrid approach to spatially distributed groundwater monitoring networks in order to reconstruct missing observations at the basin scale. Integration of reconstructed groundwater level components with GRACE/GRACE-FO—derived terrestrial water storage anomalies could improve the validation of satellite-based groundwater assessments in data-scarce regions. In addition, coupling wavelet-decomposed groundwater signals with physically based groundwater flow models may enhance long-term forecasting under changing climatic conditions. Future studies should also explore the use of advanced deep learning architectures and data assimilation techniques to better capture nonlinear interactions between climate drivers and multilayer aquifer systems.

5. Conclusions

Wavelet analysis identified three rhythmic components of GWL variability: short-, medium-, and long-period. Excluding short-period variability substantially improved the reconstruction of the principal GWL fluctuations. Long-period (multi-year) oscillations (about 5, 7–8, and 11 years and longer) dominate the long-term behavior of GWL, accounting for nearly 45% of the total signal energy. Medium-period cycles (2–4 years) represent the second most important contribution, comprising about 31% of the total energy. Thus, major shallow-groundwater trends are controlled primarily by large-scale factors and alternating dry/wet phases, with smaller contributions from local weather variability.

The results confirm that both record length and sampling frequency strongly influence wavelet decomposition outcomes and subsequent ANN reconstruction quality.

For a chronological description of GWL cycles, a Gaussian-modified wavelet periodogram is best suited, as it allows determining the start and end times of rhythms and the duration of each rhythm.

With MLP models applied to the full series (without component separation), the best reconstructions were limited to about 4 years. Longer horizons showed markedly lower accuracy. This highlights a core weakness of direct full-series ANN application: sensitivity to mixed-frequency structure and nonstationarity.

After wavelet-based decomposition into short-, medium-, and long-period components, ANN models are able to reproduce fluctuations of monthly GWL, close to the actual values for periods of up to 7 years (the best fit observed in the middle and initial sections of the modeled series, while edge effects at the end lead to a systematic overestimation or underestimation of values). That is, the decomposition method is advisable to use to fill gaps in the observation series, having previously made sure that the medium-term and long-term components make up at least 71% of the total fluctuations (see Figures S4 and S5).

Inverse wavelet reconstruction produced a GWL curve close to observations, and the reconstructed long-period behavior agrees with currently known regional GWL trends and precipitation dynamics. However, ANN-based reconstructions only complement, not replace, field measurements.

Supplementary Materials: The following supporting information can be downloaded at: https://www.mdpi.com/article/10.3390/w18172105/s1, Figure S1: Actual data on groundwater levels in wells in the Lviv region that have the longest observation series, albeit with gaps in the records, Figure S2: Comparison of GWL reconstruction results obtained using a multilayer perceptron (MLP) for well No. 51-5a (2011–2017 period) with actual data for wells No. 340005 and 368441 tapping the Upper Cretaceous aquifer (July 2017–January 2022 period), Figure S3: Extrapolation (validation test) for well UA SMS 51-5a: models were trained on data up to ~2005, and the 2006–2011 period was reconstructed. At the end of the training period, the trend was downward (−0.03 m/year), whereas during the extrapolation period, it was upward (+0.05 m/year); the short data series does not capture this long-period cycle reversal. (The extrapolation curve represents the method output; the shaded band indicates the spread of the networks), Figure S4: Reconstruction of four data gaps in the GWL dataset for well 340005 (Upper Cretaceous horizon) based on the sum of the medium-period and long-period components, Figure S5: Reconstruction of four data gaps in groundwater level (GWL) records for well 340005 (Upper Cretaceous aquifer) based on the sum of three components (including a short-period one).

Author Contributions: Conceptualization, O.S. and I.Z.; methodology, D.C. and O.S.; software, D.C.; validation, D.C., Y.S., O.S. and V.S.; formal analysis, I.Z., V.S. and O.S.; investigation, O.S., D.C. and Y.S.; resources, O.S. and I.Z.; data curation, O.S.; writing—original draft preparation, O.S. and D.C.; writing—review and editing, V.S. and I.Z.; visualization, D.C. and O.S.; supervision, O.S.; project administration, O.S.; funding acquisition, I.Z. All authors have read and agreed to the published version of the manuscript.

Funding: This research has been funded by the U.S. National Science Foundation (NSF) under the IMPRESS-U initiative, awards 2409395 and 2409396 (for the U.S. team), which unites researchers from six countries—the U.S., Ukraine, Poland, Lithuania, Latvia, and Estonia. Ukrainian project is funded by the National Academy of Sciences (NAS) and ONRG—Office of Naval Research Global, USA. Ukrainian Hydrometeorological Institute (the Ukrainian team's coordinator) receives funding from the Science and Technology Center in Ukraine (STCU), project agreement No. 7129 (1 February 2025). Vilnius University has received funding from the Research Council of Lithuania (LMTLT), agreement No. S-IMPRESSU-24-3.

Data Availability Statement: The original contributions presented in this study are included in the article. Further inquiries can be directed to the corresponding author.

Acknowledgments: This study was conducted within the international project GRANDE-U ("Groundwater Resilience Assessment through iNtegrated Data Exploration for Ukraine").

Conflicts of Interest: The authors declare no conflicts of interest.

References

1. Solovey, T.; Śliwińska-Bronowicz, J.; Janica, R.; Brzezińska, A. Terrestrial water storage changes in the Bug River Transboundary Catchment observed by GRACE and water balance analysis. *Meteorol. Hydrol. Environ. Monit.* **2024**, *2*, 4–16. [CrossRef]
2. Solovey, T.; Śliwińska-Bronowicz, J.; Janica, R.; Brzezińska, A.; Stradczuk, A. Fusing GRACE data into terrestrial water budgets to improve their predictive performance: A case study of the Bug River Transboundary Catchment, Polish-Ukrainian-Belarusian Borderland. *Geol. Q.* **2025**, *69*, 69. [CrossRef]
3. Śliwińska, J.; Birylo, M.; Rzepecka, Z.; Nastula, J. Analysis of groundwater and total water storage changes in Poland using GRACE observations, in-situ data, and various assimilation and climate models. *Remote Sens.* **2019**, *11*, 2949. [CrossRef]
4. Solovey, T.; Śliwińska-Bronowicz, J.; Janica, R.; Brzezińska, A. Assessment of the effectiveness of GRACE observations in monitoring groundwater storage in Poland. *Water Resour. Res.* **2025**, *61*, e2024WR038888. [CrossRef]
5. Rajaee, T.; Ebrahimi, H.; Nourani, V. A review of the artificial intelligence methods in groundwater level modeling. *J. Hydrol.* **2019**, *572*, 336–351. [CrossRef]
6. Wagena, M.B.; Goering, D.; Collick, A.S.; Bock, E.; Fuka, D.R.; Buda, A.; Easton, Z.M. Comparison of short-term streamflow forecasting using stochastic time series, neural networks, process-based and Bayesian models. *Environ. Model. Softw.* **2020**, *126*, 104669. [CrossRef]
7. Bikše, J.; Retike, I.; Haaf, E.; Kalvāns, A. Assessing automated gap imputation of regional scale groundwater level data sets with typical gap patterns. *J. Hydrol.* **2023**, *620*, 129424. [CrossRef]
8. Coulibaly, P.; Anctil, F.; Aravena, R.; Bobee, B. Artificial neural network modeling of water table depth fluctuations. *Water Resour. Res.* **2001**, *37*, 885–896. [CrossRef]
9. Lallahem, S.; Mania, J.; Hani, A.; Najjar, Y. On the use of neural networks to evaluate groundwater levels in fractured media. *J. Hydrol.* **2005**, *307*, 92–111. [CrossRef]
10. Feng, F.; Ghorbani, H.; Radwan, A.E. Predicting groundwater level using traditional and deep machine learning algorithms. *Front. Environ. Sci.* **2024**, *12*, 1291327. [CrossRef]
11. Daliakopoulos, I.N.; Coulibaly, P.; Tsanis, I.K. Groundwater level forecasting using artificial neural networks. *J. Hydrol.* **2005**, *309*, 229–240. [CrossRef]
12. Feng, S.; Kang, S.; Huo, Z.; Chen, S.; Mao, X. Neural networks to simulate regional groundwater levels affected by human activities. *Groundwater* **2008**, *46*, 80–90. [CrossRef]
13. Javadinejad, S.; Dara, R.; Jafary, F. How groundwater level can predict under the effect of climate change by using artificial neural networks of NARX. *Resour. Environ. Inf. Eng.* **2020**, *2*, 90–99. [CrossRef]
14. Rateb, A.; Scanlon, B.R.; Pool, D.; Sun, A.Y.; Zhang, Z.; Chen, J.; Clark, B.R.; Crilley, D.M.; Haugh, C.; Hobza, C.M.; et al. Comparison of groundwater storage changes from GRACE satellites with monitoring and modeling of major U.S. aquifers. *Water Resour. Res.* **2020**, *56*, e2020WR027556. [CrossRef]
15. Sun, A.Y. Predicting groundwater level changes using GRACE data. *Water Resour. Res.* **2013**, *49*, 5900–5912. [CrossRef]
16. Rohde, M.M.; Biswas, T.; Housman, I.W.; Campbell, L.S.; Klausmeyer, K.R.; Howard, J.K. A machine learning approach to predict groundwater levels in California reveals ecosystems at risk. *Front. Earth Sci.* **2021**, *9*, 784499. [CrossRef]
17. Eslamifar, G.; Zaslavsky, I.; Balali, H.; Samalavičius, V.; Fernald, A. Forecasting change in groundwater storage: A multilayer perceptron model leveraging system dynamics simulation data. *J. Hydrol. Reg. Stud.* **2026**, *65*, 103398. [CrossRef]
18. Samalavičius, V.; Bikše, J.; Zaslavsky, I.; Lekstutyte, I.; Arustiene, J.; Žaržojus, G.; Kunsakova, A.; Retike, I.; Gadeikiene, S.; Gadeikis, S. Sinkhole risk forecasting in the Lithuania–Latvia Karst region using artificial intelligence. *J. Hydrol. Reg. Stud.* **2026**, *65*, 103372. [CrossRef]
19. Hill, T.; O'Connor, M.; Remus, W. Neural Network Models for Time Series Forecasts. *Manag. Sci.* **1996**, *42*, 1082–1092. [CrossRef]
20. Khashei, M.; Bijari, M.; Raissi Ardali, G.A. Improvement of auto-regressive integrated moving average models using fuzzy logic and artificial neural networks (ANNs). *Neurocomputing* **2009**, *72*, 956–967. [CrossRef]
21. Guo, T.; Song, S.; Yan, Y. A time-varying autoregressive model for groundwater depth prediction. *J. Hydrol.* **2022**, *613*, 128394. [CrossRef]
22. Yurekli, K.; Kurunc, A.; Ozturk, F. Application of linear stochastic models to monthly flow data of Kelkit Stream. *Ecol. Model.* **2005**, *183*, 67–75. [CrossRef]
23. Yadav, N.; Yadav, A.; Kumar, M. *An Introduction to Neural Network Methods for Differential Equations*; Springer Briefs in Applied Science and Technology; Springer: Dordrecht, The Netherlands, 2015; pp. 17–42. [CrossRef]
24. Shevchenko, O.L.; Charnyi, D.V.; Rudoman, M.M. Forecasting groundwater flow to the Southern Bug River by statistical methods and using artificial neural networks. *Meteorol. Hydrol. Environ. Monit.* **2022**, *2*, 43–53. [CrossRef]
25. Grossmann, A.; Morlet, J. Decomposition of Hardy functions intosquare integrable wavelets of constant shape. *SIAM J. Math. Anal.* **1984**, *15*, 723–736. [CrossRef]
26. Shevchenko, O.L.; Charnyi, D.V.; Osadchyi, V.I.; Ilchenko, A.O. Groundwater runoff in the Southern Bug River basin under global warming conditions. *Geol. J.* **2021**, *3*, 3–16. [CrossRef]

27. Shevchenko, O.L.; Skorbun, A.D.; Osadchyi, V.I.; Charnyi, D.V. Changing rhythms in the groundwater regime and their relationship with climatic factors. *Bull. Taras Shevchenko Natl. Univ. Kyiv Geol.* **2021**, *2*, 71–82. [CrossRef]
28. NOAA Space Weather Prediction Center. Solar Cycle Progression and Forecast: Observed and Predicted Sunspot Numbers for Solar Cycle 25. 2026. Available online: https://www.swpc.noaa.gov/products/solar-cycle-progression (accessed on 16 December 2025).
29. Bo, Y.; Zhang, C.; Fang, X.; Sun, Y.; Li, C.; An, M.; Peng, Y.; Lu, Y. Application of HP-LSTM models for groundwater level prediction in karst regions: A case study in Qingzhen City. *Water* **2025**, *17*, 362. [CrossRef]